Letter

Anomalous Hall effect from a non-Hermitian viewpoint

Hiroki Isobe* and Naoto Nagaosa†
RIKEN Center for Emergent Matter Science (CEMS), Wako, Saitama 351-0198, Japan
and Department of Applied Physics, University of Tokyo, Bunkyo, Tokyo 113-8656, Japan

(Received 19 January 2023; revised 17 April 2023; accepted 3 May 2023; published 25 May 2023)

Non-Hermitian descriptions often model open or driven systems away from the equilibrium. Nonetheless, in equilibrium electronic systems, a non-Hermitian nature of an effective Hamiltonian manifests itself as unconventional observables such as a bulk Fermi arc and skin effects. We theoretically reveal that spin-dependent quasiparticle lifetimes, which signify the non-Hermiticity of an effective model in the equilibrium, induce the anomalous Hall effect, namely, the Hall effect without an external magnetic field. We first examine the effect of nonmagnetic and magnetic impurities and obtain a non-Hermitian effective model. Then, we calculate the Kubo formula from the microscopic model to ascertain a non-Hermitian interpretation of the longitudinal and Hall conductivities. Our results elucidate the vital role of the non-Hermitian equilibrium nature in the quantum transport phenomena.

DOI: 10.1103/PhysRevB.107.L201116

Introduction. A description of a material relies on a Hamiltonian. For an electronic system, it describes the quantum-mechanical motion of electrons under a crystalline potential. The wave function in a clean system thus has a Bloch form, consisting of a plane wave and a short-range modulation by an underlying crystal. As a wave without decay, a Bloch function represents a current with the probability conserved, which is a consequence of the Hermiticity of the Hamiltonian. In reality, however, a Bloch wave is not an exact solution in the presence of impurities or disorder. It decays during propagation, which we can effectively describe by a *non-Hermitian* Hamiltonian [1–4]. Examples of non-Hermitian effective models for quantum electronic systems include the electron-phonon coupling [5], disorder [6,7], or strong correlation [8–10]. In those systems, the non-Hermiticity causes a Fermi arc terminating with exceptional points or a drumheadlike flat band encircled by an exceptional ring [11,12]. At an exceptional point, the non-Hermitian Hamiltonian is nondiagonalizable, which never appears from a Hermitian Hamiltonian [13,14]. Despite such observable spectral features, little has been known about the role of non-Hermiticity in a nonequilibrium, in particular a quantum transport phenomenon in solids [15–17].

Non-Hermitian models appear in a variety of fields other than quantum systems [18–21], such as photonics [22–39], electrical circuits [40–43], and mechanical systems [44–56]. In classical open or driven systems, non-Hermiticity arises from gain and loss, which accompanies the energy flow in and out of the system in focus. It causes unusual features in spectrum, resonance, and propagation that never appear in a Hermitian model; e.g., sharp resonance and unidirectional transparency. Those resonance and wave propagation properties bring about advantages for measurements and detection through response of the system. Therefore, they are easily observable as opposed to the spectrum features of quantum materials.

We investigate the linear response of a two-dimensional Dirac material with impurities. We consider magnetic impurities in general, which induce *spin-dependent* scattering, and derive an effective Hamiltonian from impurity averaging. It reveals spin-dependent lifetimes leading to the non-Hermiticity. Independently, we evaluate the Kubo formula using the Dirac model with impurities by means of the conventional Feynman diagram technique. Our detailed calculations give the analytical expressions of the longitudinal and Hall conductivities, the latter of which emerges either from a uniform magnetization or randomly distributed spin-dependent impurities, along with the spin-orbit coupling embedded in the model. We reveal that the linear response properties manifest the non-Hermitian nature of the model; the spin-dependent lifetimes appearing in the effective Hamiltonian well approximate the longitudinal and Hall conductivities obtained from the Kubo formula. We also discuss the effect of skew scattering and the anomalous Hall effect induced by magnetic impurities without a uniform magnetization.

Model. We consider the Dirac Hamiltonian in two dimensions,

$$H_0(\boldsymbol{k}) = v\boldsymbol{k}\cdot\boldsymbol{\sigma} + m\sigma_z, \tag{1}$$

where the Pauli matrices σ_x, σ_y, and σ_z represent the electron's spin, and v and m are the Dirac velocity and mass, respectively. We set $\hbar = 1$ unless otherwise noted. We may regard the Hamiltonian as, e.g., a surface state of a topological insulator [57–59] with the mass m corresponding to a uniform magnetization perpendicular to the plane induced by doping or deposition. For $m = 0$, H_0 is invariant under time reversal $\mathcal{T} = i\sigma_y\mathcal{K}$ with the complex conjugation $\mathcal{K}$ as the mass m

*hiroki.isobe@riken.jp
†nagaosa@riken.jp

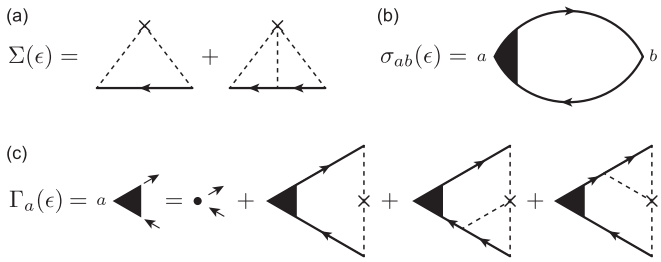

FIG. 1. Diagrammatic representations for the conductivity. (a) The self-energy captures the effect of time-reversal breaking in the effective non-Hermitian Hamiltonian. A solid line represents the Green's function $G(\boldsymbol{k}, \epsilon)$ and a cross and $p(= 2, 3)$ dashed lines correspond to the potential with the pth moment. (b) The Kubo formula calculates the longitudinal and anomalous Hall conductivities. (c) The vertex correction describes the corrections to the scattering time by impurities.

renders a uniform background magnetization coupled to Dirac electrons via the exchange coupling.

We add impurities to the clean Dirac Hamiltonian. While it is common to consider nonmagnetic potential impurities in massive models [60–65], impurities generally have potential and magnetic couplings concurrently [66–73]. In the following, we consider spin-dependent impurities, which break time-reversal symmetry, so that the clean Dirac Hamiltonian may be massless and time-reversal symmetric for a finite anomalous Hall effect. We assume here that each impurity has a magnetic moment perpendicular to the plane, which results in the impurity potential

$$H_{\rm imp}(\boldsymbol{r}) = V(\boldsymbol{r})\eta, \quad \eta = \eta_0\sigma_0 + \eta_z\sigma_z = \begin{pmatrix} \eta_{11} & 0 \\ 0 & \eta_{22} \end{pmatrix}. \quad (2)$$

Finite η_z describes the magnetic component of impurities. It breaks time-reversal symmetry microscopically while the rotational symmetry in the xy plane remains preserved. The spin-dependent impurities have a correlation between the charge (σ_0) and magnetic (σ_z) sectors. For the impurity potential $V(\boldsymbol{r})$, we consider the moments of the spatial distribution,

$$\langle V(\boldsymbol{r})V(\boldsymbol{r}')\rangle = \frac{n_i V_2}{(2\pi)^2}\delta(\boldsymbol{r}-\boldsymbol{r}'),$$
$$\langle V(\boldsymbol{r})V(\boldsymbol{r}')V(\boldsymbol{r}'')\rangle = \frac{n_i V_3}{(2\pi)^2}\delta(\boldsymbol{r}-\boldsymbol{r}')\delta(\boldsymbol{r}'-\boldsymbol{r}''), \quad (3)$$

where $\langle\cdot\rangle$ denotes impurity averaging and n_i is the impurity concentration. V_p $(p = 2, 3)$ represents a pth-order moment per single atomic potential. We set $\langle V(\boldsymbol{r})\rangle = 0$ as the uniform component merely renormalizes the chemical potential and the mass.

Self-energy with impurity averaging. We regard the impurity potential $H_{\rm imp}(\boldsymbol{r})$ as a perturbation to the clean system $H_0(\boldsymbol{k})$. We calculate the impurity average to obtain the self-energy $\Sigma^s(\epsilon)$, where $s = {\rm R(A)}$ labels the retarded (advanced) function. The self-energy follows the self-consistent equation [Fig. 1(a)], where the solid line represents the full Green's function $G^s(\boldsymbol{k}, \epsilon) = [\epsilon - H_0(\boldsymbol{k}) - \Sigma^s(\epsilon)]^{-1}$ and a cross denotes an impurity. In the following, we focus on retarded functions as Hermitian conjugation gives the corresponding advanced functions. Without spontaneous symmetry breaking of the rotational symmetry, the retarded self-energy should have the form

$$\Sigma^{\rm R}(\epsilon) = [\Sigma(\epsilon) - i\Gamma(\epsilon)]\sigma_0 + [\delta m(\epsilon) - i\gamma(\epsilon)]\sigma_z, \quad (4)$$

where $\Sigma(\epsilon)$, $\delta m(\epsilon)$, $\Gamma(\epsilon)$, and $\gamma(\epsilon)$ are real functions. We henceforth refer to $\Sigma(\epsilon)$ and $\delta m(\epsilon)$ as real parts, and $\Gamma(\epsilon)$ and $\gamma(\epsilon)$ as imaginary parts. The real parts renormalize the energy and the mass as $\bar{\epsilon}(\epsilon) = \epsilon - \Sigma(\epsilon)$ and $\bar{m}(\epsilon) = m + \delta m(\epsilon)$, respectively. We obtain the explicit form of the self-energy later.

Non-Hermitian effective Hamiltonian. We define the retarded effective Hamiltonian after impurity averaging as

$$H^{\rm R}_{\rm eff}(\boldsymbol{k}, \epsilon) = H_0(\boldsymbol{k}) + \Sigma^{\rm R}(\epsilon). \quad (5)$$

The effective Hamiltonian recovers translational symmetry, which is absent in the microscopic model due to the impurities $H_{\rm imp}(\boldsymbol{r})$. In compensation, the imaginary parts $\Gamma(\epsilon)$ and $\gamma(\epsilon)$ violate Hermiticity to describe the decay of Bloch waves. We note that Hermitian conjugation relates the retarded effective Hamiltonian not to itself but to the advanced one: $H^{\rm A}_{\rm eff}(\boldsymbol{k}, \epsilon) = [H^{\rm R}_{\rm eff}(\boldsymbol{k}, \epsilon)]^\dagger \neq H^{\rm R}_{\rm eff}(\boldsymbol{k}, \epsilon)$.

The Dirac Hamiltonian is known to host the anomalous Hall effect with a finite mass, which requires time-reversal symmetry breaking. It is beneficial to examine how the time-reversal operation $\mathcal{T} = i\sigma_y\mathcal{K}$ acts on the effective Hamiltonian. Considering that retarded and advanced functions describe forward and backward time evolutions, a necessary condition for the microscopic model to have time-reversal symmetry is $\mathcal{T}H^{\rm R}_{\rm eff}(\boldsymbol{k}, \epsilon)\mathcal{T}^{-1} = H^{\rm A}_{\rm eff}(-\boldsymbol{k}, \epsilon)$, which we dub *statistical* time-reversal symmetry for brevity [see Supplemental Material (SM) for details [74]]. In the effective Hamiltonian (5), $m(\epsilon)$ and $\gamma(\epsilon)$ break statistical time-reversal symmetry, where the former arises from a uniform magnetization and the latter from spin-dependent impurity scattering. We will see that both of them contribute to the anomalous Hall effect. We note that $\Gamma(\epsilon)$, which describes the spin-independent part of the quasiparticle lifetimes, does not break statistical time-reversal symmetry.

Despite the non-Hermitian effective Hamiltonian, we can write the Green's function in the eigenstate basis. As the effective Hamiltonian equation (5) is non-Hermitian, we have distinct left and right eigenvectors $\boldsymbol{L}_s(\boldsymbol{k}, \epsilon)$ and $\boldsymbol{R}_s(\boldsymbol{k}, \epsilon)$ with $s = \pm$ corresponding to the two complex eigenvalues $E^{\rm R}_s(\boldsymbol{k}, \epsilon) = \Sigma(\epsilon) - i\Gamma(\epsilon) + s\sqrt{v^2k^2 + [m + \delta m(\epsilon) - i\gamma(\epsilon)]^2}$ [74]. The projection operator on an eigenstate is $P_s(\boldsymbol{k}, \epsilon) = \boldsymbol{R}^T_s(\boldsymbol{k}, \epsilon)\boldsymbol{L}_s(\boldsymbol{k}, \epsilon)$. It is non-Hermitian and satisfies the completeness $\sum_{s=\pm} P_s(\boldsymbol{k}, \epsilon) = \sigma_0$. Then, we obtain the Green's function [74]

$$G^{\rm R}(\boldsymbol{k}, \epsilon) = \frac{P_+(\boldsymbol{k}, \epsilon)}{\epsilon - E^{\rm R}_+(\boldsymbol{k}, \epsilon)} + \frac{P_-(\boldsymbol{k}, \epsilon)}{\epsilon - E^{\rm R}_-(\boldsymbol{k}, \epsilon)}. \quad (6)$$

Spin-dependent lifetimes. Though a self-consistent solution requires a numerical calculation, we can analytically find a perturbative solution of the self-energy for weak impurities. As we will see later, the imaginary parts play an important role in the transport properties. The perturbative solutions of

the imaginary parts are

$$\Gamma(\epsilon) \approx \frac{\alpha_2\pi}{2}\left[\left(\eta_{11}^2+\eta_{22}^2\right)|\epsilon| + \left(\eta_{11}^2-\eta_{22}^2\right)m\,\mathrm{sgn}(\epsilon)\right] - \frac{\pi\alpha_3\Delta\Lambda}{\epsilon_0}\left[\left(\eta_{11}^3+\eta_{22}^3\right)|\epsilon| + \left(\eta_{11}^3-\eta_{22}^3\right)m\,\mathrm{sgn}(\epsilon)\right], \tag{7a}$$

$$\gamma(\epsilon) \approx \frac{\alpha_2\pi}{2}\left[\left(\eta_{11}^2-\eta_{22}^2\right)|\epsilon| + \left(\eta_{11}^2+\eta_{22}^2\right)m\,\mathrm{sgn}(\epsilon)\right] - \frac{\pi\alpha_3\Delta\Lambda}{\epsilon_0}\left[\left(\eta_{11}^3-\eta_{22}^3\right)|\epsilon| + \left(\eta_{11}^3+\eta_{22}^3\right)m\,\mathrm{sgn}(\epsilon)\right], \tag{7b}$$

for $\epsilon^2 > m^2$. Here, we introduce the dimensionless constant for the impurity strength $\alpha_p = n_i^{p/2}V_p/(4\pi v)^{p/2}$ and the energy unit $\epsilon_0 = \sqrt{4\pi v^2 n_i}$. Since we have obtained the Green's function in the eigenstate basis Eq. (6), we impose energy cutoffs separately for the conduction and valence bands, Λ_+ and Λ_-, respectively. The difference of the energy cutoffs $\Delta\Lambda = \Lambda_+ - \Lambda_-$ appears at order α_3. We retain the terms at order α_3 because $\alpha_3\Delta\Lambda/\epsilon_0$ can be comparable to α_2 even for $|\alpha_3| \ll \alpha_2$ [74].

Importantly, the present impurity model generates spin-dependent lifetimes, defined by the imaginary part of the self-energy as

$$\tau_\uparrow = \frac{1}{2(\Gamma+\gamma)}, \quad \tau_\downarrow = \frac{1}{2(\Gamma-\gamma)}. \tag{8}$$

$\gamma(\epsilon)$ represents their difference, and importantly, it arises regardless of a uniform magnetization but by impurities with $\eta_{11} \neq \eta_{22}$, when the impurity scattering depends on spin. We note that the relation $\Gamma(\epsilon) \geqslant |\gamma(\epsilon)|$ must hold as the system is not driven by an external force. In other words, the two lifetimes are positive and hence quasiparticles always decay.

Conductivity calculations. Now we calculate the conductivity σ_{ab} $(a, b = x, y)$ from the microscopic model $H_0 + H_{\mathrm{imp}}$ using the Kubo formula. It is convenient to decompose the formula as in the Kubo-Středa formula [75,76], which leads to analytic solutions. At zero temperature [77], we write the electric conductivity at the Fermi level ϵ as $\sigma_{ab}(\epsilon) = \sigma_{ab}^{(\mathrm{Ia})}(\epsilon) + \sigma_{ab}^{(\mathrm{Ib})}(\epsilon) + \sigma_{ab}^{(\mathrm{II})}(\epsilon)$ [Fig. 1(b)], where the three terms are $\sigma_{ab}^{(\mathrm{Ia})}(\epsilon) = \int_{\boldsymbol{k}} \mathrm{tr}[j_a G^{\mathrm{R}}(\epsilon) j_b G^{\mathrm{A}}(\epsilon)]/(2\pi)$, $\sigma_{ab}^{(\mathrm{Ib})}(\epsilon) = -\int_{\boldsymbol{k}} \mathrm{tr}\left[\, j_a G^{\mathrm{R}}(\epsilon) j_b G^{\mathrm{R}}(\epsilon) + j_a G^{\mathrm{A}}(\epsilon) j_b G^{\mathrm{A}}(\epsilon)\,\right]/(4\pi)$, and $\sigma_{ab}^{(\mathrm{II})}(\epsilon) = \int_{\boldsymbol{k}} \int_{-\infty}^{\epsilon} d\epsilon'\, \mathrm{tr}[j_a G^{\mathrm{R}}(\epsilon') j_b \partial_{\epsilon'} G^{\mathrm{R}}(\epsilon') - j_a \partial_{\epsilon'} G^{\mathrm{R}}(\epsilon') j_b G^{\mathrm{R}}(\epsilon') + j_a \partial_{\epsilon'} G^{\mathrm{A}}(\epsilon') j_b G^{\mathrm{A}}(\epsilon') - j_a G^{\mathrm{A}}(\epsilon') j_b \partial_{\epsilon'} G^{\mathrm{A}}(\epsilon')]/(4\pi)$ with $\int_{\boldsymbol{k}} = \int d^2k/(2\pi)^2$. We omit $\boldsymbol{k}$ in the Green's function and the trace acts on the Pauli matrices for spin. j_a is the current operator and its bare form without impurity scattering is $j_a = -ev\sigma_a$. Since we include the effect of scattering in the Green's function as a self-energy, we need to incorporate the vertex correction for a self-consistent calculation [78]. In the following, we discuss the calculation of the conductivity at a low impurity concentration, i.e., consider an expansion with respect to n_i. Then, we should retain the vertex correction in $\sigma_{ab}^{(\mathrm{Ia})}$ while those in $\sigma_{ab}^{(\mathrm{Ib})}$ and $\sigma_{ab}^{(\mathrm{II})}$ give higher-order corrections [61]. We should thus replace one current operator j_a in $\sigma_{ab}^{(\mathrm{Ia})}$ with $j_a = -ev\Gamma_a(\epsilon)$, which we should determine according to the self-consistent equation [Fig. 1(c)] [74].

By evaluating the Kubo formula, we obtain the analytic expression of the conductivity [74]

$$\sigma_{ab}^{(\mathrm{Ia})}(\epsilon) = \frac{e^2}{4\pi^2}[\boldsymbol{\Gamma}(\epsilon)\boldsymbol{\Lambda}(\epsilon)]_{ab}, \quad \sigma_{ab}^{(\mathrm{Ib})}(\epsilon) = \frac{e^2}{4\pi^2}\delta_{ab}, \tag{9a}$$

$$\sigma_{ab}^{(\mathrm{II})}(\epsilon) = -\frac{e^2}{4\pi^2}\varepsilon_{abz}\,\mathrm{Im}\,\ln\frac{\bar\epsilon - \bar m + i\Gamma + i\gamma}{\bar\epsilon + \bar m + i\Gamma - i\gamma}. \tag{9b}$$

The matrices $\boldsymbol{\Gamma}(\epsilon)$ and $\boldsymbol{\Lambda}(\epsilon)$ are related to the vertex and ladder functions:

$$\boldsymbol{\Gamma} = \{\mathbf{1} - \alpha_2\eta_{11}\eta_{22}\boldsymbol{\Lambda} - \alpha_3\eta_{11}\eta_{22} \times \left[(\eta_{11}+\eta_{22})\,\mathrm{Re}\,I_0^{\mathrm{R}} + (\eta_{11}-\eta_{22})\,\mathrm{Re}\,I_z^{\mathrm{R}}\right]\boldsymbol{\Lambda} - \alpha_3\eta_{11}\eta_{22} \times \left[(\eta_{11}-\eta_{22})\,\mathrm{Im}\,I_0^{\mathrm{R}} + (\eta_{11}+\eta_{22})\,\mathrm{Im}\,I_z^{\mathrm{R}}\right]\boldsymbol{\Lambda}\boldsymbol{\varepsilon}\}^{-1}, \tag{10}$$

$$\boldsymbol{\Lambda} = \frac{\mathrm{Im}\,\ln\zeta}{\mathrm{Im}\,\zeta}[(\bar\epsilon^2 + \Gamma^2 - \bar m^2 - \gamma^2)\mathbf{1} - 2(\bar m\Gamma + \bar\epsilon\gamma)\boldsymbol{\varepsilon}], \tag{11}$$

where we use $(\mathbf{1})_{ab} = \delta_{ab}$ and $(\boldsymbol{\varepsilon})_{ab} = \varepsilon_{zab}$ with the Levi-Civita symbol ε_{abc}. We also define the functions $\zeta(\epsilon) = (\bar m - i\gamma)^2 - (\bar\epsilon + i\Gamma)^2$ and

$$I_0^{\mathrm{R}}(\epsilon) = -\frac{\Delta\Lambda}{\epsilon_0} - \frac{\bar\epsilon + i\Gamma}{\epsilon_0}\ln\frac{\Lambda_+\Lambda_-}{\zeta}, \tag{12a}$$

$$I_z^{\mathrm{R}}(\epsilon) = -\frac{\bar m - i\gamma}{\epsilon_0}\ln\frac{\Lambda_+\Lambda_-}{\zeta}. \tag{12b}$$

We note that $\boldsymbol{\Gamma}(\epsilon)$, $\boldsymbol{\Lambda}(\epsilon)$, and $I_{0,z}^{\mathrm{R}}(\epsilon)$ are dimensionless functions.

$\sigma_{ab}^{(\mathrm{Ib})}$ contributes only to the longitudinal conductivity and $\sigma_{ab}^{(\mathrm{II})}$ to the Hall conductivity. Roughly speaking, the Hall conductivity inside the band gap ($\bar\epsilon^2 < \bar m^2$) comes from $\sigma_{ab}^{(\mathrm{II})}$ to give $\sigma_{xy} \approx -e^2/(2h)$ with the Planck constant $h(= 2\pi\hbar)$ recovered. For large doping $|\epsilon| \gg |m|, \epsilon_0$, $\sigma_{ab}^{(\mathrm{Ia})}$ predominantly contributes to the conductivity. For $|\alpha_3| \ll \alpha_2$ when skew scattering is not dominant, we find the approximate forms

$$\sigma_{xx}(\epsilon) \approx \frac{e^2}{8\pi}\frac{|\epsilon|}{\Gamma(\epsilon)}\phi, \tag{13a}$$

$$\sigma_{xy}(\epsilon) \approx -\frac{e^2}{4\pi}\frac{\gamma(\epsilon)}{\Gamma(\epsilon)}\phi^2\,\mathrm{sgn}(\epsilon). \tag{13b}$$

The constant $\phi = [1 - \eta_{11}\eta_{22}/(\eta_{11}^2 + \eta_{22}^2)]^{-1}$ originates from the vertex correction and hence characterizes transport quantities. From $\sigma_{xx}(\epsilon)$, we can identify $\tau_{\mathrm{tr}}(\epsilon) = \phi/[2\Gamma(\epsilon)]$ as the transport scattering time [79,80]. On the other hand, it is worth emphasizing that the approximate form of the anomalous Hall conductivity σ_{xy} relies on $\gamma(\epsilon)$. We recall that a finite $\gamma(\epsilon)$ manifests the spin-dependent lifetimes ($\tau_\uparrow \neq \tau_\downarrow$) and the absence of time-reversal symmetry of the impurity model in the equilibrium. Using $\tau_{\uparrow,\downarrow}$, we find $\sigma_{xy} \propto (\tau_\uparrow - \tau_\downarrow)/(\tau_\uparrow + \tau_\downarrow)$ along with the spin-orbit coupling embedded in the Dirac model. The approximate forms, Eqs. (13), provide a non-Hermitian interpretation of the electric conductivity for both longitudinal and transverse components.

Numerical results. We show the longitudinal conductivity σ_{xx} and the Hall conductivity σ_{xy} in Fig. 2. We evaluate the analytic expressions of the conductivity Eq. (9) with the self-energy numerically obtained from the self-consistent equation [Fig. 1(a)]. We use the conductivity unit $e^2/(2\pi\hbar) =$

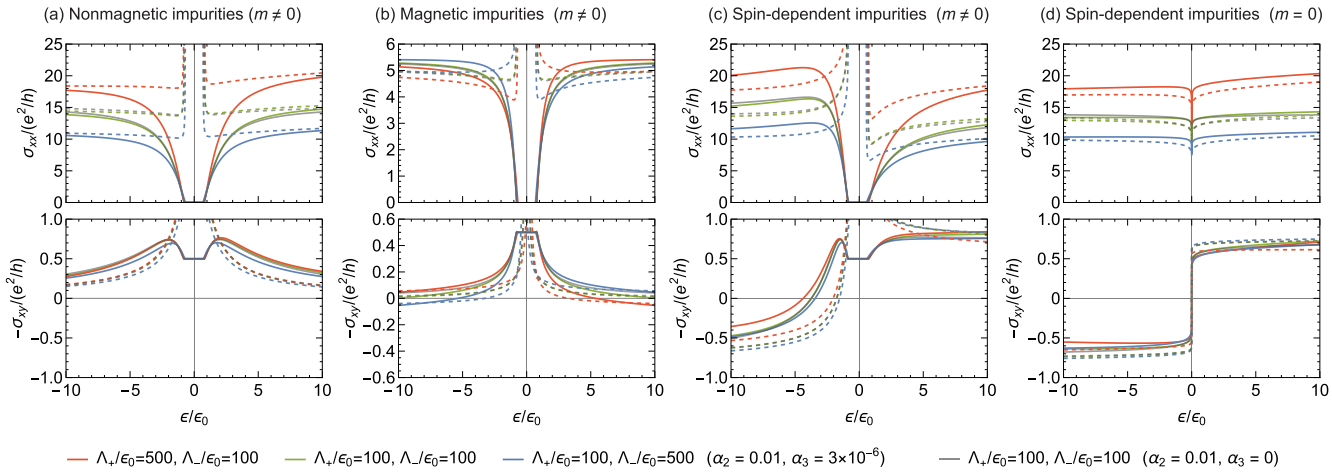

FIG. 2. Fermi level dependence of the conductivity. The upper panels show the longitudinal conductivity σ_{xx} and the lower panels the Hall conductivity σ_{xy}. (a)–(d) correspond to different impurity spin components and masses: (a) $\eta = \sigma_0$ (nonmagnetic), $m = \epsilon_0$ (massive); (b) $\eta = \sigma_z$ (magnetic), $m = \epsilon_0$ (massive); (c) $\eta_{11} = \sqrt{3/2}$, $\eta_{22} = \sqrt{1/2}$ (spin dependent), $m = \epsilon_0$ (massive); and (d) $\eta_{11} = \sqrt{3/2}$, $\eta_{22} = \sqrt{1/2}$ (spin dependent), $m = 0$ (massless). We keep $\eta_{11}^2 + \eta_{22}^2$ constant for all cases. We choose the dimensionless constants for the impurity strength as $\alpha_2 = 0.01$, $\alpha_3 = 3 \times 10^{-6}$ for the colored lines, while the gray lines correspond to the cases without skew scattering $\alpha_2 = 0.01$, $\alpha_3 = 0$. Different colors represent different energy cutoffs; see the legend. The cutoff dependence is as weak as logarithmic for $\alpha_3 = 0$. The solid lines represent the exact solutions, Eq. (9), and the dashed lines the approximate results with a non-Hermitian interpretation, Eq. (13).

e^2/h with the Planck constant h recovered. We present the results for various impurity types, masses, and energy cutoffs. We also depict the approximate results of Eqs. (13) in the same figure using the dashed lines, revealing a good agreement at relatively large doping from the Dirac point. It corroborates the non-Hermitian interpretation of the longitudinal and Hall conductivities. The approximation deviates from the self-consistent solution for $|\epsilon| \lesssim |m|$, which coincides with the region where the semiclassical approximation breaks down.

The dimensionless parameter α_3 characterizes the skewness of the impurity potential distribution whereas α_2 characterizes the impurity potential strength. We note that α_3 is a major source of skew scattering [81,82]. With the symmetric energy cutoffs for the conduction and valence bands ($\Delta\Lambda = 0$), the effect of skewness is tiny with the ratio $\alpha_3/\alpha_2^2 = 0.04$; compare the green and gray lines in Fig. 2. Its dependence is as weak as logarithmic, which we can infer from Eq. (12). However, asymmetric cutoffs ($\Delta\Lambda \neq 0$) enhance the effect of skewness (red and blue lines in Fig. 2) as it appears with a potentially large factor $\Delta\Lambda/\epsilon_0$ in the self-energy Eq. (7) and the vertex correction Eq. (10). They modify the conductivity through the quasiparticle lifetime and the scattering time, respectively.

Now we discuss the effect of the magnetic properties of impurities. For nonmagnetic impurities [Fig. 2(a)], our result coincides with the previous result with symmetric energy cutoffs [61,64,65,74]. In this case, a uniform magnetization that yields a finite mass breaks time-reversal symmetry to induce finite anomalous Hall effect. The skewness α_3 makes the conductivity asymmetric about the charge neutrality $\epsilon = 0$ as it breaks electron-hole symmetry. We observe a larger conductivity in the conduction band where $\alpha_3\eta_0\epsilon > 0$, because the scattering amplitude by an impurity is smaller when the impurity potential is repulsive [65,83]. Also, we tend to observe a larger conductivity for $\Lambda_+ > \Lambda_-$, when the band in which the impurity potential is repulsive has a wider energy range. The peak structure of the conductivity implies broad resonance of scattering [65], which is contained in the vertex correction, Eq. (10), in the present analysis. For magnetic impurities [Fig. 2(b)], the conductivity is reduced compared to the nonmagnetic impurity case with the same potential strength. Here we observe certain electron-hole symmetry, which we will discuss later.

In reality, a magnetic impurity induces both potential and magnetic scatterings at a single site ($\eta_0, \eta_z \neq 0$); in other words, impurity scattering becomes spin dependent [Fig. 2(c)]. Then, the anomalous Hall effect appears even without a uniform magnetization $m = 0$ [Fig. 2(d)]. The magnetism of impurities imparts time-reversal symmetry breaking, giving rise to δm and γ [see Eq. (7) and SM [74]]. The effect is prominent and realistic for $\eta_0, \eta_z \neq 0$ while purely magnetic impurities ($\eta_0 = 0$, $\eta_z \neq 0$) without magnetization ($m = 0$) can generate finite σ_{xy} with $\alpha_3 \neq 0$ [74]. The longitudinal conductivity shows a weak dependence on the Fermi level with a sharp dip at $\epsilon = 0$ to $\sigma_{xx} \simeq e^2/(2\pi^2)$ [74].

Symmetries. Some numerical results are symmetric or antisymmetric about the charge neutrality ($\epsilon = 0$), which we can understand from the symmetries of the model. We consider the following three symmetry operations: (i) time reversal $\mathcal{T} = i\sigma_y\mathcal{K}$, (ii) charge conjugation $\mathcal{C} = \sigma_x\mathcal{K}$, and (iii) their product $\mathcal{S} = \mathcal{T}\mathcal{C} = \sigma_z$. For convenience, we refer to $\mathcal{S}$ as "sublattice" symmetry [84]. $\mathcal{S}$ is a local operation acting on a spin, which we may view as reflection ($z \mapsto -z$) about the two-dimensional system embedded in a three-dimensional space for the present model. The clean Hamiltonian $H_0(\boldsymbol{k})$ has electron-hole symmetry

$$\mathcal{C}H_0(\boldsymbol{k})\mathcal{C}^{-1} = -H_0(-\boldsymbol{k}), \tag{14a}$$

while the impurity potential transforms as

$$\mathcal{C}V(\boldsymbol{r})(\eta_0\sigma_0 + \eta_z\sigma_z)\mathcal{C}^{-1} = -V(\boldsymbol{r})(-\eta_0\sigma_0 + \eta_z\sigma_z). \tag{14b}$$

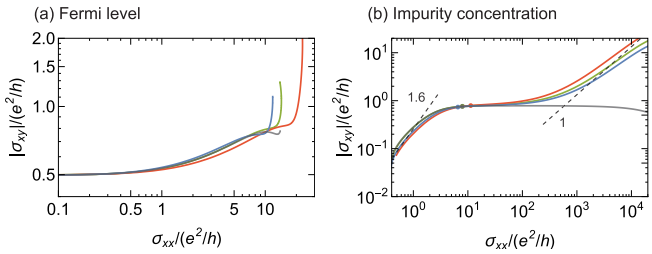

FIG. 3. Scaling relations between the longitudinal and Hall conductivities. We use the same color scheme as that of Fig. 2. We show the scaling plots by varying (a) the Fermi level ($0 < \epsilon/\epsilon_0 < 100$) and (b) the impurity concentration n_i at $\epsilon/\epsilon_0 = 3$. We choose spin-dependent impurities ($\eta_{11} = \sqrt{3/2}$, $\eta_{22} = \sqrt{1/2}$) and the mass $m = \epsilon_0$. (a) corresponds to the positive energy region in Fig. 2(c), and the points in (b) indicate the impurity concentration used in Fig. 2(c).

If $\eta_0 = 0$, the entire system preserves electron-hole symmetry $\mathcal{C}(H_0 + H_{\rm imp})\mathcal{C}^{-1} = -(H_0 + H_{\rm imp})$. Therefore, the conductivity with magnetic impurities is symmetric about the charge neutrality as we have seen in Fig. 2(b). The operator $\mathcal{C}$ swaps the energy cutoffs for the conduction and valence bands as well. For $\eta_0 \neq 0$ and $\eta_z = 0$, the conductivity remains electron-hole symmetric if $\alpha_3 = 0$, since the distribution of the impurity potential retains electron-hole symmetry [see gray lines in Fig. 2(a)]. In other words, converting $V(\boldsymbol{r})$ to $-V(\boldsymbol{r})$ does not change α_2; i.e., electron-hole symmetry is statistically preserved.

In the gapless case, on the other hand, $\mathcal{S}$ transforms the Hamiltonian as

$$\mathcal{S}H_0(\boldsymbol{k})\mathcal{S}^{-1} = -H_0(\boldsymbol{k}) \quad (m = 0), \tag{15a}$$

$$\mathcal{S}H_{\rm imp}(\boldsymbol{r})\mathcal{S}^{-1} = H_{\rm imp}(\boldsymbol{r}). \tag{15b}$$

If $\alpha_3 = 0$, the model statistically preserves the "electron-hole" symmetry imposed by $\mathcal{S}$. As $\mathcal{S}$ is virtually a reflection about the plane, the Hall conductivity changes sign under $\mathcal{S}$ and hence it becomes antisymmetric about the charge neutrality whereas the longitudinal conductivity remains symmetric [Fig. 2(d)]. See SM for more details [74].

Scaling. Figure 3 shows the scaling plots by varying the Fermi level ϵ and the impurity concentration n_i. For other parameters, we use the same values as those for Fig. 2(c). When we increase the Fermi level from the band edge [Fig. 3(a)], the longitudinal conductivity σ_{xx} gradually increases while the Hall conductivity σ_{xy} remains around $e^2/(2h)$. For $e^2/h \lesssim \sigma_{xx} \lesssim 10e^2/h$, there seems a scaling region with $|\sigma_{xy}| \propto \sigma_{xx}^{0.2}$ [74]. As σ_{xx} grows, it begins to saturate because of the artifact of short-range impurities [80], but σ_{xy} keeps growing linearly with the energy owing to skew scattering [74], resulting in a rapid upturn in the scaling plot. On the other hand, the scaling plot by varying the impurity concentration reveals the known behavior. As σ_{xx} increases with smaller n_i, we observe the side-jump, intrinsic, and skew-scattering regions, where we find the approximate scaling relations $|\sigma_{xy}| \propto \sigma_{xx}^{1.6}$, $|\sigma_{xy}| \sim$ const, and $|\sigma_{xy}| \propto \sigma_{xx}^{1}$, respectively [60].

Discussions. In Fig. 2(d), we observed the anomalous Hall effect in the absence of a uniform magnetization ($m = 0$). It relies on the spin-dependent scattering ($\eta_0, \eta_z \neq 0$), leading to spin-dependent lifetimes $\tau_\uparrow \neq \tau_\downarrow$ and thus non-Hermiticity of the effective model. In reality, random magnetic impurities may have a finite uniform magnetization considering that the magnetic component η_z arises from the exchange coupling. We note that the gapped and gapless cases [Figs. 2(c) and 2(d)] are continuously connected. In addition, one might concern the violation of the Onsager reciprocal relation, when the Hall conductivity is finite without a uniform magnetization. However, finite anomalous Hall effect requires magnetic impurities, which microscopically break time-reversal symmetry, so that our results comply with the Onsager reciprocal relation. Lastly, it is worth pointing out that the gapless Dirac model does not have a finite Berry curvature, so that it is natural to attribute finite σ_{xy} to scattering-related phenomena rather than the intrinsic origin.

Acknowledgments. This work was supported by JST CREST Grant No. JPMJCR1874, Japan, and JSPS KAKENHI Grant No. 18H03676.

[1] N. Hatano and D. R. Nelson, Localization Transitions in Non-Hermitian Quantum Mechanics, Phys. Rev. Lett. **77**, 570 (1996).
[2] N. Hatano and D. R. Nelson, Vortex pinning and non-Hermitian quantum mechanics, Phys. Rev. B **56**, 8651 (1997).
[3] C. M. Bender and S. Boettcher, Real Spectra in Non-Hermitian Hamiltonians Having $\mathcal{PT}$ Symmetry, Phys. Rev. Lett. **80**, 5243 (1998).
[4] C. M. Bender, Making sense of non-Hermitian Hamiltonians, Rep. Prog. Phys. **70**, 947 (2007).
[5] V. Kozii and L. Fu, Non-hermitian topological theory of finite-lifetime quasiparticles: Prediction of bulk Fermi arc due to exceptional point, arXiv:1708.05841.
[6] M. Papaj, H. Isobe, and L. Fu, Nodal arc of disordered Dirac fermions and non-Hermitian band theory, Phys. Rev. B **99**, 201107(R) (2019).
[7] A. A. Zyuzin and A. Yu. Zyuzin, Flat band in disorder-driven non-Hermitian Weyl semimetals, Phys. Rev. B **97**, 041203(R) (2018).
[8] T. Yoshida, R. Peters, and N. Kawakami, Non-Hermitian perspective of the band structure in heavy-fermion systems, Phys. Rev. B **98**, 035141 (2018).
[9] K. Kimura, T. Yoshida, and N. Kawakami, Chiral-symmetry protected exceptional torus in correlated nodal-line semimetals, Phys. Rev. B **100**, 115124 (2019).
[10] Y. Nagai, Y. Qi, H. Isobe, V. Kozii, and L. Fu, DMFT Reveals the Non-Hermitian Topology and Fermi Arcs in Heavy-Fermion Systems, Phys. Rev. Lett. **125**, 227204 (2020).
[11] H. Shen, B. Zhen, and L. Fu, Topological Band Theory for Non-Hermitian Hamiltonians, Phys. Rev. Lett. **120**, 146402 (2018).

[12] E. J. Bergholtz, J. C. Budich, and F. K. Kunst, Exceptional topology of non-Hermitian systems, Rev. Mod. Phys. **93**, 015005 (2021).

[13] T. Kato, *Perturbation Theory for Linear Operators*, Classics in Mathematics (Springer, New York, 1995).

[14] W. D. Heiss, The physics of exceptional points, J. Phys. A **45**, 444016 (2012).

[15] Y. Michishita and R. Peters, Effects of renormalization and non-Hermiticity on nonlinear responses in strongly correlated electron systems, Phys. Rev. B **103**, 195133 (2021).

[16] B. Michen and J. C. Budich, Mesoscopic transport signatures of disorder-induced non-Hermitian phases, Phys. Rev. Res. **4**, 023248 (2022).

[17] Y. Michishita and N. Nagaosa, Dissipation and geometry in nonlinear quantum transports of multiband electronic systems, Phys. Rev. B **106**, 125114 (2022).

[18] N. Moiseyev, *Non-Hermitian Quantum Mechanics*, (Cambridge University Press, Cambridge, UK, 2011).

[19] I. Rotter, A non-Hermitian Hamilton operator and the physics of open quantum systems, J. Phys. A: Math. Theor. **42**, 153001 (2009).

[20] D. C. Brody, Biorthogonal quantum mechanics, J. Phys. A: Math. Theor. **47**, 035305 (2014).

[21] Y. Ashida, Z. Gong, and M. Ueda, Non-Hermitian physics, Adv. Phys. **69**, 249 (2020).

[22] A. Guo, G. J. Salamo, D. Duchesne, R. Morandotti, M. Volatier-Ravat, V. Aimez, G. A. Siviloglou, and D. N. Christodoulides, Observation of $\mathcal{PT}$-Symmetry Breaking in Complex Optical Potentials, Phys. Rev. Lett. **103**, 093902 (2009).

[23] Z. Lin, H. Ramezani, T. Eichelkraut, T. Kottos, H. Cao, and D. N. Christodoulides, Unidirectional Invisibility Induced by $\mathcal{PT}$-Symmetric Periodic Structures, Phys. Rev. Lett. **106**, 213901 (2011).

[24] L. Feng, Y.-L. Xu, W. S. Fegadolli, M.-H. Lu, J. E. B. Oliveira, V. R. Almeida, Y.-F. Chen, and A. Scherer, Experimental demonstration of a unidirectional reflectionless parity-time metamaterial at optical frequencies, Nat. Mater. **12**, 108 (2013).

[25] A. Regensburger, C. Bersch, M.-A. Miri, G. Onishchukov, D. N. Christodoulides, and U. Peschel, Parity–time synthetic photonic lattices, Nature (London) **488**, 167 (2012).

[26] B. Peng, Ş. K. Özdemir, F. Lei, F. Monifi, M. Gianfreda, G. L. Long, S. Fan, F. Nori, C. M. Bender, and L. Yang, Parity–time-symmetric whispering-gallery microcavities, Nat. Phys. **10**, 394 (2014).

[27] J. Wiersig, Sensors operating at exceptional points: General theory, Phys. Rev. A **93**, 033809 (2016).

[28] W. Chen, Ş. K. Özdemir, G. Zhao, J. Wiersig, and L. Yang, Exceptional points enhance sensing in an optical microcavity, Nature (London) **548**, 192 (2017).

[29] H. Hodaei, A. U. Hassan, S. Wittek, H. Garcia-Gracia, R. El-Ganainy, D. N. Christodoulides, and M. Khajavikhan, Enhanced sensitivity at higher-order exceptional points, Nature (London) **548**, 187 (2017).

[30] M. P. Hokmabadi, A. Schumer, D. N. Christodoulides, and M. Khajavikhan, Non-Hermitian ring laser gyroscopes with enhanced Sagnac sensitivity, Nature (London) **576**, 70 (2019).

[31] B. Zhen, C. W. Hsu, Y. Igarashi, L. Lu, I. Kaminer, A. Pick, S.-L. Chua, J. D. Joannopoulos, and M. Soljačić, Spawning rings of exceptional points out of Dirac cones, Nature (London) **525**, 354 (2015).

[32] H. Zhou, C. Peng, Y. Yoon, C. W. Hsu, K. A. Nelson, L. Fu, J. D. Joannopoulos, M. Soljačić, and B. Zhen, Observation of bulk Fermi arc and polarization half charge from paired exceptional points, Science **359**, 1009 (2018).

[33] A. Cerjan, S. Huang, M. Wang, K. P. Chen, Y. Chong, and M. C. Rechtsman, Experimental realization of a Weyl exceptional ring, Nat. Photonics **13**, 623 (2019).

[34] M. Brandstetter, M. Liertzer, C. Deutsch, P. Klang, J. Schöberl, H. E. Türeci, G. Strasser, K. Unterrainer, and S. Rotter, Reversing the pump dependence of a laser at an exceptional point, Nat. Commun. **5**, 4034 (2014).

[35] H. Xu, D. Mason, L. Jiang, and J. G. E. Harris, Topological energy transfer in an optomechanical system with exceptional points, Nature (London) **537**, 80 (2016).

[36] H. Zhao, X. Qiao, T. Wu, B. Midya, S. Longhi, and L. Feng, Non-Hermitian topological light steering, Science **365**, 1163 (2019).

[37] S. Weidemann, M. Kremer, T. Helbig, T. Hofmann, A. Stegmaier, M. Greiter, R. Thomale, and A. Szameit, Topological funneling of light, Science **368**, 311 (2020).

[38] R. El-Ganainy, K. G. Makris, M. Khajavikhan, Z. H. Musslimani, S. Rotter, and D. N. Christodoulides, Non-Hermitian physics and PT symmetry, Nat. Phys. **14**, 11 (2018).

[39] M.-A. Miri and A. Alù, Exceptional points in optics and photonics, Science **363**, eaar7709 (2019).

[40] T. Hofmann, T. Helbig, C. H. Lee, M. Greiter, and R. Thomale, Chiral Voltage Propagation and Calibration in a Topolectrical Chern Circuit, Phys. Rev. Lett. **122**, 247702 (2019).

[41] M. Ezawa, Electric circuits for non-Hermitian Chern insulators, Phys. Rev. B **100**, 081401(R) (2019).

[42] T. Helbig, T. Hofmann, S. Imhof, M. Abdelghany, T. Kiessling, L. W. Molenkamp, C. H. Lee, A. Szameit, M. Greiter, and R. Thomale, Generalized bulk–boundary correspondence in non-Hermitian topolectrical circuits, Nat. Phys. **16**, 747 (2020).

[43] T. Hofmann, T. Helbig, F. Schindler, N. Salgo, M. Brzezińska, M. Greiter, T. Kiessling, D. Wolf, A. Vollhardt, A. Kabaši, C. H. Lee, A. Bilušić, R. Thomale, and T. Neupert, Reciprocal skin effect and its realization in a topolectrical circuit, Phys. Rev. Res. **2**, 023265 (2020).

[44] R. Fleury, D. Sounas, and A. Alù, An invisible acoustic sensor based on parity-time symmetry, Nat. Commun. **6**, 5905 (2015).

[45] K. G. Makris, Z. H. Musslimani, D. N. Christodoulides, and S. Rotter, Constant-intensity waves and their modulation instability in non-Hermitian potentials, Nat. Commun. **6**, 7257 (2015).

[46] K. Ding, G. Ma, M. Xiao, Z. Q. Zhang, and C. T. Chan, Emergence, Coalescence, and Topological Properties of Multiple Exceptional Points and Their Experimental Realization, Phys. Rev. X **6**, 021007 (2016).

[47] K. G. Makris, A. Brandstötter, P. Ambichl, Z. H. Musslimani, and S. Rotter, Wave propagation through disordered media without backscattering and intensity variations, Light Sci. Appl. **6**, e17035 (2017).

[48] E. Rivet, A. Brandstötter, K. G. Makris, H. Lissek, S. Rotter, and R. Fleury, Constant-pressure sound waves in non-Hermitian disordered media, Nat. Phys. **14**, 942 (2018).

[49] C. Shi, M. Dubois, Y. Chen, L. Cheng, H. Ramezani, Y. Wang, and X. Zhang, Accessing the exceptional points of parity-time symmetric acoustics, Nat. Commun. **7**, 11110 (2016).

[50] Y. Aurégan and V. Pagneux, $\mathcal{PT}$-Symmetric Scattering in Flow Duct Acoustics, Phys. Rev. Lett. **118**, 174301 (2017).

[51] M. Brandenbourger, X. Locsin, E. Lerner, and C. Coulais, Non-reciprocal robotic metamaterials, Nat. Commun. **10**, 4608 (2019).

[52] C. Scheibner, W. T. M. Irvine, and V. Vitelli, Non-Hermitian Band Topology and Skin Modes in Active Elastic Media, Phys. Rev. Lett. **125**, 118001 (2020).

[53] D. Zhou and J. Zhang, Non-Hermitian topological metamaterials with odd elasticity, Phys. Rev. Res. **2**, 023173 (2020).

[54] M. I. N. Rosa and M. Ruzzene, Dynamics and topology of non-Hermitian elastic lattices with non-local feedback control interactions, New J. Phys. **22**, 053004 (2020).

[55] H. Schomerus, Nonreciprocal response theory of non-Hermitian mechanical metamaterials: Response phase transition from the skin effect of zero modes, Phys. Rev. Res. **2**, 013058 (2020).

[56] A. Ghatak, M. Brandenbourger, J. van Wezel, and C. Coulais, Observation of non-Hermitian topology and its bulk–edge correspondence in an active mechanical metamaterial, Proc. Natl. Acad. Sci. USA **117**, 29561 (2020).

[57] X.-L. Qi, T. L. Hughes, and S.-C. Zhang, Topological field theory of time-reversal invariant insulators, Phys. Rev. B **78**, 195424 (2008).

[58] To relate Hamiltonian equation (1) to a surface state of a topological insulator, e.g., Bi_2Te_3, we may need a spin rotation in the xy plane, which does not alter the discussion.

[59] L. Fu, Hexagonal Warping Effects in the Surface States of the Topological Insulator Bi_2Te_3, Phys. Rev. Lett. **103**, 266801 (2009).

[60] S. Onoda, N. Sugimoto, and N. Nagaosa, Intrinsic Versus Extrinsic Anomalous Hall Effect in Ferromagnets, Phys. Rev. Lett. **97**, 126602 (2006).

[61] N. A. Sinitsyn, A. H. MacDonald, T. Jungwirth, V. K. Dugaev, and J. Sinova, Anomalous Hall effect in a two-dimensional Dirac band: The link between the Kubo-Streda formula and the semiclassical Boltzmann equation approach, Phys. Rev. B **75**, 045315 (2007).

[62] N. A. Sinitsyn, Semiclassical theories of the anomalous Hall effect, J. Phys.: Condens. Matter **20**, 023201 (2008).

[63] N. Nagaosa, J. Sinova, S. Onoda, A. H. MacDonald, and N. P. Ong, Anomalous Hall effect, Rev. Mod. Phys. **82**, 1539 (2010).

[64] T. Ando, Theory of valley Hall conductivity in graphene with gap, J. Phys. Soc. Jpn. **84**, 114705 (2015).

[65] T. Ando, Valley Hall conductivity in graphene: Effects of higher-order scattering, J. Phys. Soc. Jpn. **87**, 044702 (2018).

[66] J. Inoue, T. Kato, Y. Ishikawa, H. Itoh, G. E. W. Bauer, and L. W. Molenkamp, Vertex Corrections to the Anomalous Hall Effect in Spin-Polarized Two-Dimensional Electron Gases with a Rashba Spin-Orbit Interaction, Phys. Rev. Lett. **97**, 046604 (2006).

[67] T. Kato, Y. Ishikawa, H. Itoh, and J. Inoue, Anomalous Hall effect in spin-polarized two-dimensional electron gases with Rashba spin–orbit interaction, New J. Phys. **9**, 350 (2007).

[68] T. S. Nunner, N. A. Sinitsyn, M. F. Borunda, V. K. Dugaev, A. A. Kovalev, Ar. Abanov, C. Timm, T. Jungwirth, J. Inoue, A. H. MacDonald, and J. Sinova, Anomalous Hall effect in a two-dimensional electron gas, Phys. Rev. B **76**, 235312 (2007).

[69] T. S. Nunner, G. Zaránd, and F. von Oppen, Anomalous Hall Effect in a Two Dimensional Electron Gas with Magnetic Impurities, Phys. Rev. Lett. **100**, 236602 (2008).

[70] S. A. Yang, H. Pan, Y. Yao, and Q. Niu, Scattering universality classes of side jump in the anomalous Hall effect, Phys. Rev. B **83**, 125122 (2011).

[71] A. C. Keser, R. Raimondi, and D. Culcer, Sign Change in the Anomalous Hall Effect and Strong Transport Effects in a 2D Massive Dirac Metal Due to Spin-Charge Correlated Disorder, Phys. Rev. Lett. **123**, 126603 (2019).

[72] R. Wakatsuki, M. Ezawa, and N. Nagaosa, Domain wall of a ferromagnet on a three-dimensional topological insulator, Sci. Rep. **5**, 13638 (2015).

[73] H. Isobe and N. Nagaosa, Quantum Transport and Magnetism of Dirac Electrons in Solids, Phys. Rev. Lett. **129**, 216601 (2022).

[74] See Supplemental Material at http://link.aps.org/supplemental/10.1103/PhysRevB.107.L201116 for the details about the non-Hermitian effective Hamiltonian, the calculation of the conductivity, and the symmetries of the model, which includes Refs. [60,61,78,85].

[75] P. Streda, Theory of quantised Hall conductivity in two dimensions, J. Phys. C **15**, L717 (1982).

[76] A. Crépieux and P. Bruno, Theory of the anomalous Hall effect from the Kubo formula and the Dirac equation, Phys. Rev. B **64**, 014416 (2001).

[77] Finite temperature smears the energy dependence and the conductivity becomes $\int d\epsilon[-f'(\epsilon)]\sigma_{ab}(\epsilon)$, where $f(\epsilon)$ is the Fermi-Dirac distribution function.

[78] D. Vollhardt and P. Wölfle, Diagrammatic, self-consistent treatment of the Anderson localization problem in $d \leqslant 2$ dimensions, Phys. Rev. B **22**, 4666 (1980).

[79] K. Nomura and A. H. MacDonald, Quantum Hall Ferromagnetism in Graphene, Phys. Rev. Lett. **96**, 256602 (2006).

[80] T. Stauber, N. M. R. Peres, and F. Guinea, Electronic transport in graphene: A semiclassical approach including midgap states, Phys. Rev. B **76**, 205423 (2007).

[81] J. Smit, The spontaneous Hall effect in ferromagnetics I, Physica **21**, 877 (1955).

[82] J. Smit, The spontaneous Hall effect in ferromagnetics II, Physica **24**, 39 (1958).

[83] D. S. Novikov, Elastic scattering theory and transport in graphene, Phys. Rev. B **76**, 245435 (2007).

[84] S. Ryu, A. P. Schnyder, A. Furusaki, and A. W. W. Ludwig, Topological insulators and superconductors: Tenfold way and dimensional hierarchy, New J. Phys. **12**, 065010 (2010).

[85] P. M. Ostrovsky, I. V. Gornyi, and A. D. Mirlin, Electron transport in disordered graphene, Phys. Rev. B **74**, 235443 (2006).